journal

J. Am. Ceram. Soc., 88 [7] 1981–1984 (2005)
DOI: 10.1111/j.1551-2916.2005.00260.x

Synthesis and Characterization of Nano-Hetero-Structured Dy Doped CeO_2 Solid Electrolytes Using a Combination of Spark Plasma Sintering and Conventional Sintering

Toshiyuki Mori,[†] Tomoaki Kobayashi,[‡] and Yarong Wang

Ecomaterials Center, National Institute for Materials Science, Tsukuba, Ibaraki 305-0044, Japan

John Drennan

Centre for Microscopy and Microanalysis, The University of Queensland, Brisbane, St. Lucia 4072, Australia

Toshiyuki Nishimura and Ji-Guang Li

Advanced Materials Laboratory, National Institute for Materials Science, Tsukuba, Ibaraki 305-0044, Japan

Hidehiko Kobayashi

Faculty of Engineering, Saitama University, Saitama City, Saitama 338-8570, Japan

Doped ceria (CeO_2) compounds are fluorite-type oxides that show oxide ionic conductivity higher than yttria-stabilized zirconia in oxidizing atmosphere. As a consequence of this, considerable interest has been shown in application of these materials for "low" (500°–650°C) temperature operation of solid oxide fuel cells (SOFCs). To improve the conductivity in dysprosium (Dy) doped CeO_2, nano-size round shape particles were prepared using a coprecipitation method. The dense sintered bodies with small grain sizes (<300 nm) were fabricated using a combined process of spark plasma sintering (SPS) and conventional sintering (CS). Dy-doped CeO_2 sintered body with large grains (1.1 μm) had large micro-domains. The conductivity in the sintered body was low (−3.2 S/cm at 500°C). On the other hand, the conductivity in the specimens obtained by the combined process was considerably improved. The micro-domain size in the grain was minimized using the present process. It is concluded that the enhancement of conductivity in dense specimens produced by the combined process (SPS+CS) is attributable to the microstructural changes within the grains.

I. Introduction

Oxide ion conductors are used in a variety of oxygen sensors,[1–3] solid oxide electrochemical cells,[4–6] and solid oxide fuel cells (SOFCs).[7–9] In these applications, SOFCs are being especially developed as a clean and efficient power source for generating electricity from a variety of fuels. Doped CeO_2 compounds such as Gd-doped CeO_2[10–12] and Sm-doped CeO_2[13–16] are now under active investigations for application as "low" (500°–650°C) temperature operation of SOFCs. These electrolytes show high oxide ionic conductivity at high oxygen partial pressure. At low oxygen partial pressures associated with anodic conditions, these materials are partially reduced and develop electronic conductivity during operation of the fuel cell. To overcome this problem and improve the conductivity for low temperature operation of SOFCs, the influence of nano-structural feature in the doped CeO_2 systems on the conducting property should be taken into account. It is expected from the growing body of information that a new conduction pathway will come to light in nano-structured solid electrolytes. As a consequence, a new design paradigm is required to produce nano-structured doped CeO_2 electrolytes.

Spark plasma sintering (SPS) is a sintering method that allows a quick densification utilizing the microscopic electrical discharges that occur between particles that are under pressure and that are simultaneously subjected to an applied electric current. This sintering method is useful for preparation of nano-structured oxide composites,[17–20] and oxide-nonoxide composites.[21–24] However, SPS has not been applied to fabricate the dense sintered bodies of rare earth-doped CeO_2 electrolytes. The reason for this is that carbon penetration from the graphite die into the specimen was observed to prevent the densification of the sample. In this communication, the combined process of SPS and conventional sintering (CS) was used to prepare dense dysprosium (Dy) doped CeO_2 with nano-hetero structure. The densification behavior, conducting properties, and microstructure at the atomic level of dense specimens prepared in this manner were examined with a view to finding new ways of improving the conducting properties of Dy-doped CeO_2. The influence of microstructural features on conductivities in (SPS+CS) specimens was compared with those prepared by conventional means.

II. Experimental Procedure

The starting materials used for Dy-doped CeO_2 synthesis were cerium nitrate hexahydrate ($Ce(NO_3)_3 \cdot 6H_2O$; >99.99% pure, KANTO Chemical Co. Inc., Tokyo, Japan), dysprosium nitrate hexahydrate ($Dy(NO_3)_3 \cdot 6H_2O$; >99.9% pure, Wako Pure Chemical Industries Inc., Osaka, Japan), and ammonium carbonate ($(NH_4)_2CO_3$; ultrahigh purity, KANTO Chemical Co. Inc.). The cerium nitrate hexahydrate and dysprosium nitrate hexahydrate powders were dissolved in distilled water, and the solutions were mixed in order to prepare the composition of $Dy^{3+}/Ce^{3+} = 1/4$. An aqueous solution of ammonium carbonate in distilled water with a concentration of 1.5*M* was used

D. W. Johnson Jr.—contributing editor

Manuscript No. 11066. Received May 26, 2004; approved November 15, 2004.
[†]Author to whom correspondence should be addressed. e-mail: mori.toshiyuki@nims.go.jp
[‡]Faculty of Engineering, Saitama University, Saitama City, Saitama 338-8570, Japan.

as the precipitant. The mixed solution was added into the ammonium carbonate solution kept at 70°C while being gently stirred. After repeated washing, the precipitate was dried at room temperature with flowing nitrogen gas and then calcined in flowing oxygen at 700°C for 2 h to yield doped CeO_2 powders. For CS, these powders were molded under a pressure of 500 kg/cm^2 and subjected to a rubber press at 2 t/cm^2 (1 t = 10^3kg) in order to obtain a green body. CS temperature ranged from 1000° to 1450°C for 4–6 h. In the combined process, a two-step sintering process was performed. The first step uses the SPS that is followed in the second step by CS. For SPS, 2 g of the powders were placed into a 15 mm graphite die and an electric current of 1000 A was applied under a pressure of 60 MPa. The heating rate was 500°C/min. The sintering temperature ranged from 1000° to 1200°C. To minimize the penetration of carbon from the graphite die into the specimens, no holding time at the aforementioned sintering temperature was used. The current was simply shut off at temperature and the pressure was immediately released after the sintering. Following the SPS process, the specimens were sintered at the temperature ranging from 1000° to 1200°C for up to 48 h in air.

The crystal phases in the powder and sintered specimens were investigated using X-ray diffraction and selected area electron diffraction analysis, respectively. The bulk density of the sintered body was measured using the Archimedes method. The relative density was calculated from the ratio of the measured bulk density to the theoretical density. The theoretical density was estimated using the lattice constant and the sample composition. The particle sizes in the synthesized powders and the grain sizes in the sintered bodies were observed using scanning electron microscopy (SEM). The average grain size in the sintered body was calculated using the linear intercept method measuring more than 200 grains using SEM.[25] The microstructural features in the grain were investigated in detail using transmission electron microscopy (TEM). Ion beam thinned specimens were used for TEM observation. In order to avoid reduction of CeO_2 by ion beam milling, Ar ion beam was irradiated using cooled cold stage in liquid nitrogen. TEM observation was performed with gun voltages of 200 keV.

For the electrical conductivity measurement, platinum electrodes were applied to both sides of the sintered bodies at 1000°C. The conducting properties in the sintered bodies were measured by dc three point measurements at 400°–650°C in air. The accuracy of conductivity in each temperature is ± 0.01 S/cm in log σ.

III. Results and Discussion

Figure 1 shows morphology of the powders calcined at 700°C for 2 h. The CeO_2 powder doped with Dy^{3+} is observed to be composed of uniformly sized, round shaped, and discrete particles. The average particle size was approximately 20 nm. This powder can be sintered to over 95% dense of theoretical density (7.327 g/cm^3) in the temperature range of 1100°–1450°C using CS methods as described. On the other hand, SPS could not make dense Dy-doped CeO_2 sintered bodies over 95% of theoretical one. It is because the carbon powders penetrated the sintered body from the graphite die and lowered the bulk density of the specimen. The maximum bulk density of SPS specimen was approximately 85% of theoretical one. To make sintered body with high density over 95%, the combined process of SPS and CS was examined.

Figure 2 presents the relationship between the sintering time of CS after SPS and the relative density. The relative density of Dy-doped CeO_2 specimens reached 95% of theoretical density using the combined process of SPS and CS. On the other hand, the powder of Dy-doped CeO_2 that was obtained from a solid-state reaction of oxide powders, CeO_2 and Dy_2O_3, showed a poor sintering property. Its relative density was 75% of theoretical one using the combined process of SPS (1200°C, no holding time) and CS (1100°C, 24 h). This suggests that the fine Dy-doped CeO_2 powder is required for fabrication of a dense sintered body using the present combined process of SPS and CS.

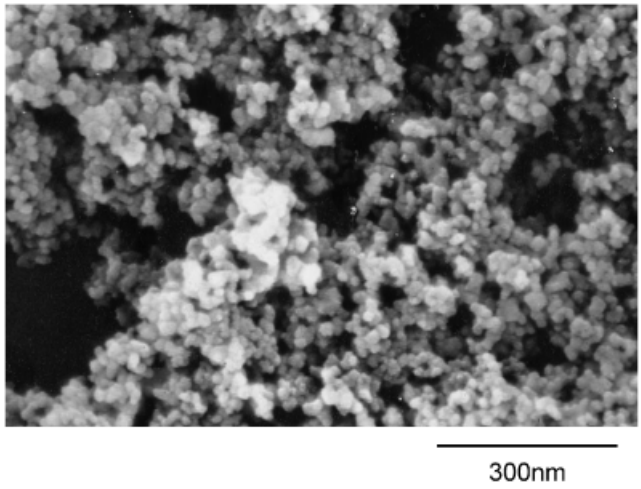

Fig. 1. Scanning electron microscopy photograph of $Dy_{0.2}Ce_{0.8}O_{1.9}$ powder. Calcination temperature: 700°C; holding time: 2 h.

Figure 3 shows the relationship between conductivity, activation energy, and grain size in the Dy-doped CeO_2 sintered bodies that were obtained by CS and combined process of SPS and CS. The conductivity in the specimens that were obtained by CS showed the curvature in the grain size dependence of conductivity (Fig. 3(a)). The conductivity decreased with decreasing grain size and reached the lowest value at an average grain size of 240 nm. This tendency would be attributable to the space charge layer around the grain boundary in the sintered body. On the other hand, the conductivity increased with a decrease of grain size under 240 nm. In this region, it is suggested that the space charge layer with high resistivity is minimized around the grain boundary. Since the change of conductivity is large when the grains are below 240 nm, then we suggest it is not all attributable to space charge changes. Other microstructural features within the grain are also beginning to have an influence. Both change of the space charge layer width around grain boundary and the microstructural features within the grain would lead to improvements in the conductivity that are observed in the sintered bodies.

In order to improve the conductivity in this grain size region, the combined process of SPS and CS was examined. As Fig. 3(a) indicates, the conductivity in the sintered body with small grain

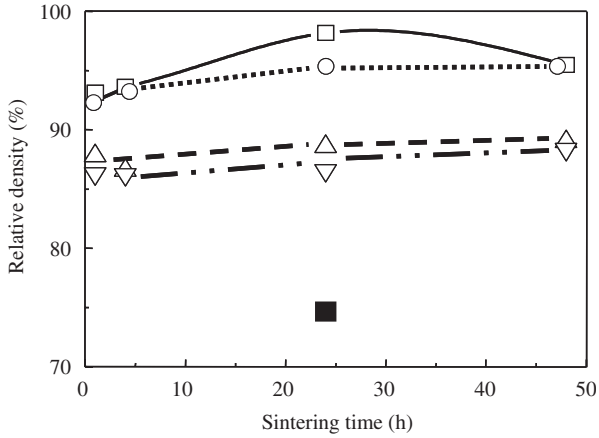

Fig. 2. Relationship between relative density and sintering time of conventional sintering (CS) after spark plasma sintering (SPS); the relative density of specimen obtained by SPS: 85% of theoretical density. CS temperature: ▽, 1000°C; △, 1050°C; ○, 1100°C; □, 1150°C. Closed symbol means the relative density of specimen obtained by solid-state reaction powder; ■, 1150°C.

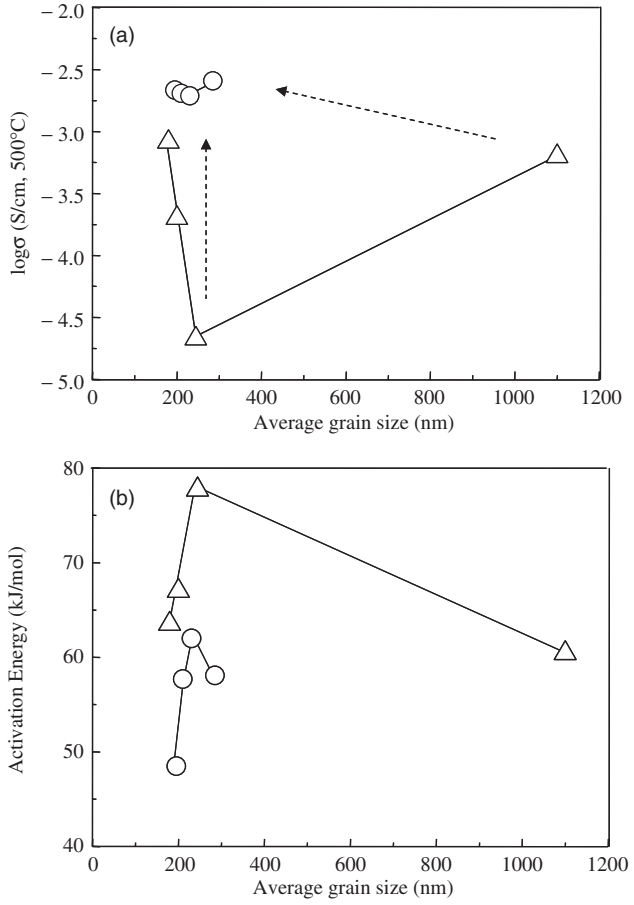

Fig. 3. Electrolytic properties in $Dy_{0.2}Ce_{0.8}O_{1.9}$ sintered bodies obtained by conventional sintering (CS) or (spark plasma sintering (SPS)+CS). (a) Conductivity versus average grain size. ○, (SPS+CS) specimen; △, CS specimen. (b) Activation energy versus average grain size. ○, (SPS+CS) specimen; △, CS specimen.

(approximately 240 nm) was drastically improved by the present combined process. The activation energy in the specimens, which were prepared using CS, has a clear maximum in the graph showing the relationship between activation energy and grain size. The maximum point is equal to the minimum point of conductivity as shown in Fig. 3(b). In addition, the activation energy in the specimens obtained by the combined method of SPS and CS was much lower than that of the specimens prepared by CS. This suggests that microstructures in aforementioned specimens are more than superficially different and the microstructure in the grain is more complex and may provide the key to developing high conducting properties.

Figure 4(a) displays the selected area electron diffraction pattern and high-resolution image recorded from the sintered body with the average grain size of 1.1 μm (1100 nm) that was obtained by CS. The diffuse scattering exists in the background of electron diffraction pattern. This indicates that micro-domain with coherent interface is present in the grain. In addition, very small extra spots that are indicated by dashed arrow lines coexisted with main fluorite-type spots in the electron diffraction pattern. These extra spots, which can be indexed on a distorted pyrochlore structure, suggest that coherent domains of this structural arrangement exist in this material as shown in the calculated electron diffraction pattern (Fig. 4(b)). In general, the Dy^{3+} is known to replace Ce^{4+} and create oxygen vacancies. However, it is known that segregation of dopant cations to the grain boundary region occurs. The lattice distortion would be introduced into fluorite lattice by this segregation. To minimize the lattice distortion in CeO_2 lattice, micro-domain with ordered structure would be formed in the lattice. The micro-domain

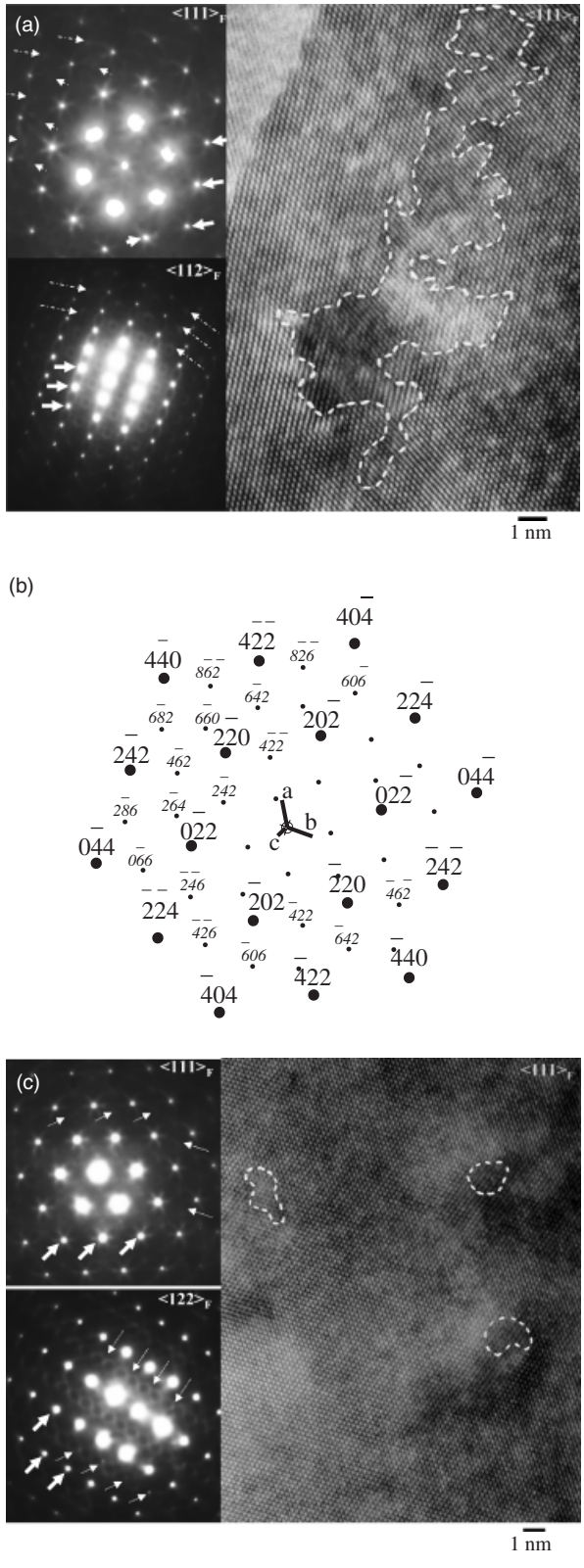

Fig. 4. (a) Selected area electron diffraction patterns ($\langle 111\rangle_F$, $\langle 112\rangle_F$) and high-resolution image ($\langle 111\rangle_F$) recorded from $Dy_{0.2}Ce_{0.8}O_{1.9}$ sintered body (grain size: 1.1 μm) obtained by conventional sintering (CS), dashed area is micro-domain. (b) Calculated electron diffraction pattern of fluorite $[111]_F$+distorted pyrochlore $[111]_P$, large circle indicates fluorite pattern, small circle indicates pyrochlore pattern. (c) Selected area electron diffraction patterns ($\langle 111\rangle_F$, $\langle 122\rangle_F$) and high resolution image ($\langle 111\rangle_F$) recorded from $Dy_{0.2}Ce_{0.8}O_{1.9}$ sintered body (grain size: 290 nm) obtained by (spark plasma sintering+CS), F means fluorite and P means pyrochlore, dashed area is micro-domain. Dashed arrow line indicates extra reflection. Solid arrow line indicates fluorite spot.

would be developed in the grain to minimize this lattice distortion. The size of micro-domain was over 10 nm. Some micro-domains combined with each other to become the continuous micro-domain with irregular shapes. In the nano-sized grain of the specimens fabricated by CS, it is concluded that the micro-domain size is minimized by the small segregation and the low space charge layer level.

On the other hand, the specimen obtained by the combined process of SPS and CS has different nano-hetero structure as compared with aforementioned specimen. Figure 4(c) displays the selected area electron diffraction pattern and high-resolution image recorded from the sintered body with the average grain size of 240 nm that was obtained by the combined process of SPS and CS. The diffuse scattering was observed in the background of electron diffraction pattern, but the intensity of the extra reflection is weak. The high-resolution image indicates that the growth of micro-domain in the specimen was suppressed and the size of micro-domain is under 2 nm. This suggests that the present combined process lowers the heterogeneity in the grain. Also, the proposed combined process minimizes the size of micro-domain and improves the conducting property in the specimen. While this microstructural change is subtle, the nano-hetero structure with nano-size domain in the grain has a significant influence on the electrolytic properties. We believe that the design of nano-hetero structure with nano-size domain is a key for improvement of conducting property in doped ceria electrolytes.

IV. Summary

The effect of combined process of SPS and CS on the design of nano-hetero structure in Dy-doped CeO_2 solid electrolyte was examined. Round shape Dy-doped CeO_2 powders were prepared using carbonate coprecipitation method. Dense sintered bodies (over 95% of theoretical density) were obtained using the present process. The fine powder was required for the fabrication of dense sintered body in this process. The specimen obtained by CS had continuous micro-domain with distorted pyrochlore structure or its related structure. On the other hand, the size of micro-domain was minimized in the specimens that were prepared using the combined process of SPS and CS. Accordingly, the design of nano-hetero structure is very important for improvement of conducting property in doped CeO_2 solid electrolytes.

References

[1]N. Yamazoe and N. Miura, "Gas Sensors Using Solid Electrolytes," *MRS Bull.*, **24** [6] 37–43 (1999).

[2]U. Nigge, H. D. Wiemhofer, E. W. J. Romer, H. J. M. Bouwmeester, and T. R. Schulte, "Composites of $Ce_{0.8}Gd_{0.2}O_{1.9}$ and $Gd_{0.7}Ca_{0.3}CoO_{3-x}$ as Oxygen Permeable Membranes for Exhaust Gas Sensors," *Solid State Ionics*, **146** [1–2] 163–74 (2002).

[3]A. Hashimoto, T. Hibino, and M. Sano, "Fuel Cell Type Sensor for Detection of Carbon Monoxide in Reformed Gases," *Electrochem. Solid State Lett.*, **5** [2] H1–3 (2002).

[4]M. Stoukides and C. G. Vayenus, "The Effect of Electrochemical Oxygen Pumping on the Rate and Selectivity of Ethylene Oxidation on Polycrystalline Silver," *J. Catal.*, **70**, 137–46 (1981).

[5]S. Hamakawa, T. Hayakawa, A. P. E. York, T. Tsunoda, Y. S. Yoon, K. Suzuki, M. Shimizu, and K. Takehira, "Selective Oxidation of Propene Using an Electrochemical Membrane Reactor with CeO_2 Based Solid Electrolyte," *J. Electrochem. Soc.*, **143** [4] 1264–8 (1996).

[6]T. Hibino, K. Ushiki, Y. Kuwahara, and M. Mizuno, "Electrochemical Removal of NO and CH_4 in the Presence of Excess O_2, H_2O, and CO_2 Using Sm_2O_3 Doped CeO_2 as a Solid Electrolyte," *J. Chem. Soc.-Faraday Trans.*, **92** [21] 4297–300 (1996).

[7]N. Q. Minh, "Ceramic Fuel Cells," *J. Am. Ceram Soc.*, **76**, 563–88 (1993).

[8]S. C. Singhal, "Science and Technology of Solid Oxide Fuel Cells," *MRS Bull.*, **25** [3] 16–21 (2000).

[9]B. C. H. Steel, "Materials for Fuel-Cell Technologies," *Nature*, **414** [15] 345–52 (2001).

[10]T. Kudo and H. Obayashi, "Mixed Electrical Conduction in Fluorite-Type $Ce_{1-x}Gd_xO_{2-x/2}$," *J. Electrochem. Soc.*, **123** [3] 415–9 (1976).

[11]B. C. H. Steel, "Appraisal of $Ce_{1-y}Gd_yO_{2-y/2}$ Electrolytes for IT-SOFC Operation at 500°C," *Solid State Ionics*, **129**, 95–110 (2000).

[12]R. Doshi, V. L. Richards, J. D. Carter, X. Wang, and M. Krumpelt, "Development of Solid Oxide Fuel Cells That Operate at 500°C," *J. Electrochem. Soc.*, **146** [4] 1273–8 (1999).

[13]M. Gödickemeier and L. J. Gauckler, "Engineering of Solid Oxide Fuel Cells with Ceria Based Electrolytes," *J. Electrochem. Soc.*, **145** [2] 414–21 (1998).

[14]C. Milliken, S. Guruswamy, and A. Khandkar, "Evaluation of Ceria Electrolytes in Solid Oxide Fuel Cells Electric Power Generation," *J. Electrochem. Soc.*, **146** [3] 872–82 (1999).

[15]C. Milliken, S. Guruswamy, and A. Khandkar, "Properties and Performance of Cation Doped Ceria Electrolyte Materials in Solid Oxide Fuel Cell Applications," *J. Am. Ceram. Soc.*, **85** [10] 2479–86 (2002).

[16]C. Lu, W. L. Worrell, R. J. Gorte, and J. M. Vohs, "SOFCs for Direct Oxidation of Hydrocarbon Fuels with Samaria Doped Ceria Electrolyte," *J. Electrochem. Soc.*, **150** [3] A354–8 (2003).

[17]L. Gao, J. S. Hong, H. Miyamoto, and S. D. De La Torre, "Superfast Densification of Oxide Ceramics by Spark Plasma Sintering," *J. Inorg. Mater.*, **13** [1] 18–22 (1998).

[18]L. Gao, Z. J. Shen, H. Miyamoto, and M. Nygren, "Superfast Densification of Oxide/Oxide Ceramics Composites," *J. Am. Ceram. Soc.*, **82** [4] 1061–3 (1999).

[19]K. A. Khor, L. G. Yu, Z. L. Dong, and Z. A. Munir, "Spark Plasma Reaction Sintering of ZrO_2-Mullite Composites from Plasma Spheroidized Zircon/Alumina Powders," *Mater. Sci. Eng. A-Struct. Mater. Properties, Microstruct. Process.*, **339** [1–2] 286–96 (2003).

[20]H. B. Gao, K. A. Khor, Y. C. Boey, and X. G. Miao, "Laminated and Functionally Graded Hydoxyapatite/Yttria Stabilized Tetragonal Zirconia Composites Fabricated by Spark Plasma Sintering," *Biomaterials*, **24** [4] 667–75 (2003).

[21]L. Gao, H. Z. Wang, J. S. Hong, H. Miyamoto, K. Miyamoto, Y. Nishikawa, and S. D. De La Torre, "SiC-ZrO_2(3Y)-Al_2O_3 Nano-Composites Superfast Densification by Spark Plasma Sintering," *Nanostruct. Mater.*, **11** [1] 43–9 (1999).

[22]L. A. Gao, X. H. Jin, H. Kawaoka, T. Sekino, and K. Niihara, "Microstructure and Mechanical Properties of SiC-Mullite Nanocomposite Prepared by Spark Plasma Sintering," *Mater. Sci. Eng. A-Struct. Mater. Properties, Microstruct. Process.*, **334** [1–2] 262–6 (2002).

[23]G. D. Zhan, J. D. Kuntz, J. L. Wan, and A. K. Mukherjee, "Single-Wall Carbon Nanotubes as Attractive Toughening Agents in Alumina-Based Nanocomposites," *Nat. Mater.*, **2** [1] 38–42 (2003).

[24]G. D. Zhan, J. D. Kuntz, J. E. Garay, and A. K. Mukherjee, "Electrical Properties of Nanoceramics Reinforced with Ropes of Single-Walled Carbon Nanotubes," *Appl. Phys. Lett.*, **83** [6] 1228–30 (2003).

[25]M. I. Mendelson, "Average Grain Size in Polycrystalline Ceramics," *J. Am. Ceram. Soc.*, **52** [8] 443–6 (1969). □